ACS Photonics

Article

pubs.acs.org/journal/apchd5

Loop-Turn Optical Flows with Spectral Selectivity in Suspended Plasmonic Nanofin-Cavity Structure

Ya-Lun Ho,[†] Minoru Abasaki,[‡] and Jean-Jacques Delaunay*[,†]

[†]Department of Mechanical Engineering, School of Engineering, The University of Tokyo, 7-3-1 Hongo, Bunkyo-ku, Tokyo 113-8656, Japan

[‡]Fuji Electric Co., Ltd., 1 Fujimachi, Hino-shi, Tokyo 191-8502, Japan

Supporting Information

ABSTRACT: Metallic nanostructures sustain surface plasmons that strongly couple incident light to the surface of the metal. They have received a great amount of attention as a possible means of light manipulation. Among the various reported structures, cavities are promising for spectroscopic applications because the cavity mode, with its narrow band, large modulation, and tunability over a wide range of wavelengths, provides a means to improve the resonances in far-field measurements. This report describes a suspended plasmonic nanofin-cavity structure capable of producing tunable reflected resonances with high quality factors (Q) in the infrared (IR) region. The nanofin-cavity structure having plasmonic hot spots on the ridges supports standing-wave resonances with enhanced electric fields in the horizontal and vertical directions; strong optical flows are thus generated and light turns in a loop, resulting in high reflectance. When the nanofin cavity is further coupled to the propagating surface plasmon resonance (SPR), a strong and narrow-band reflectance resonance due to the stringent condition of SPR arises with a bandwidth having a full width at half-maximum (FWHM) of 92 nm and a Q as large as 60. Furthermore, as result of the coupled modes, the intensity of the resonance peak depends on the angle of the incident light and thus presents a potential means of angle-controlled optical switching in the IR region. Finally, high-order modes of a nanofin-cavity structure were observed in the near-infrared (NIR) region for which wavelengths are much shorter than the cavity scale, thus, demonstrating the possibility of easing the difficulty of fabrication.

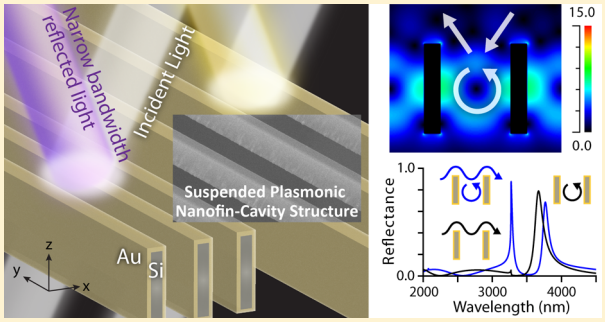

KEYWORDS: *plasmonics, optical flows, nanocavities, coupling, infrared filters, nanophotonics*

Surface plasmons are collective oscillations of electrons on an interface between a metal and a dielectric that are generated from the interaction of light and the metal, and they have been of growing interest because of the possibility of creating nanostructures that use them to manipulate light.[1−12] By utilizing such a plasmonic structure, light can be manipulated on the subwavelength scale, which overcomes the limitation of conventional optics.[13,14] Metallic nanoholes, nanoslits, and metal−insulator−metal structures have the ability to transmit light. These nanostructures are able to tune the transmission peak in the visible region and have been proposed as band-pass filters.[15−22] In contrast, other plasmonic waveguide structures have been demonstrated as band-stop filters.[23−26] However, the resonances of these plasmonic nanostructures are broad, and the absorption of the metal layers weakens the resonance. As a result, compared with silicon (Si) photonic microcavities having resonances with extremely high Q factors,[27,28] metallic nanostructures generally have much lower Q factors due to decay of the electric field in the metal materials.[29−32] Moreover, the resonance can only be controlled in a limited range of the visible or NIR region, and it is difficult to obtain a strong and narrow-band resonance with a long wavelength in the IR region, which would be of use in probing the fingerprint region of organic molecules.

Here, a three-dimensional suspended nanofin-cavity structure consisting of metal-coated nanofins was designed and fabricated. Due to the coupling of plasmonic hot spots to the nanofin cavities, strong optical flows turning light in a loop are sustained in the nanofin cavities and the optical properties of the nanofin-cavity structure change from being highly transparent to highly reflective at the resonance wavelength. Therefore, strong and tunable reflected resonances are realized in a very wide range from the NIR to IR region. This characteristic is different from most band-pass filters based on light transmission and emitters[33,34] supporting strong light confinement. The relatively large spaces between the nanofins in our structure are utilized to form the loop-turn optical flow, which supports narrow-band light reflection instead of strong confinement and transmission. Nanofin structures having smaller spaces between nanofins and strong field confinement were reported in our previous reports.[35,36] Furthermore, by

Received: February 24, 2015
Published: May 7, 2015

DOI: 10.1021/acsphotonics.5b00083
ACS Photonics 2015, 2, 730−737

coupling nanofin cavities and the propagating SPR, the bandwidth of the reflected resonances can be narrowed because of the stringent SPR condition. A strong reflectance band can be tuned by varying the period of the nanofin cavities, and this presents a promising way to manipulate the nanofin cavities through the use of microsystems taking advantage of the suspended nanofin-cavity structure. The characteristics of the nanofin-cavity structure provide a new way to design band-pass filters, optical switches, sensor, and applications in the fingerprint region.

The nanofin-cavity structure consists of Si nanofins aligned in parallel and coated with a gold (Au) layer. The schematic diagram is presented in Figure 1a,b, together with the

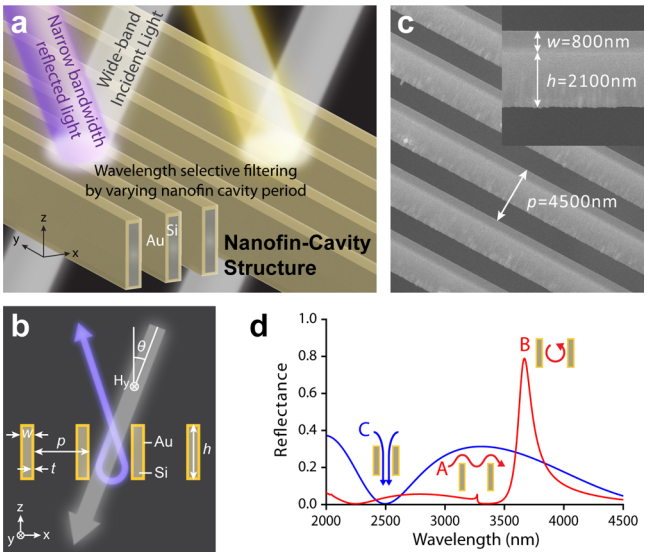

Figure 1. (a) Illustration of the nanofin-cavity structure. (b) Schematic cross-section of the nanofin-cavity structure together with the cavity parameters and the direction and polarization of the incident light. The gray arrow represents the wide-band incident light with high transmittance except for the light at a specific wavelength (the purple arrow) which turns in a loop resulting in high reflectance. The parameters are the period of the cavity p, the height of the nanofin h, the width of Au-coated Si nanofins w, the thickness of the Au layer t, and the incident angle θ. (c) Electron microscopy images of the fabricated nanofin-cavity structure with a tilted view at 45°. The inset shows a magnified view. (d) Simulated reflection spectra with periodic boundary conditions for p = 2600 (red) and 1000 nm (blue), w = 500 nm, h = 2200 nm, and t = 100 nm at θ = 15°.

parameters, namely, the period of the cavities p, the width of the nanofins w, the height of the nanofins h, and the thickness of the Au layer t. The structure is surrounded by air (refractive index n = 1) with p-polarized light incident at an angle θ. A fabricated suspended nanofin cavity is shown in Figure 1c. The period, height, and width of the nanofin cavities are measured from the tilted view electron microscopy images. Simulated zero-order reflection spectra are presented in Figure 1d for structures having p = 2600 and 1000 nm, w = 500 nm, h = 2200 nm, and t = 100 nm at θ = 15° (curves in red and blue, respectively). The simulation used rigorous coupled-wave analysis (DiffractMOD, Rsoft Design Group, Ossining, U.S.A.). The blue reflectance curve shows the typical light properties without a sharp resonance. The broad dip of the low reflectance represents the light transmission of the structure; that is, light passes through the nanofin cavities. A small-modulation peak (Point A) at 3273 nm and a large-modulation peak (Point B) at 3671 nm in the red curve are for reflectances of 0.05 and 0.79, respectively. The small-modulation peak represents propagating SPR and agrees well with the excitation condition:[37]

$$\frac{2\pi}{\lambda}\sqrt{\varepsilon_1}\sin\theta + N\frac{2\pi}{p} = \pm\frac{2\pi}{\lambda}\sqrt{\varepsilon_1\varepsilon_2/(\varepsilon_1+\varepsilon_2)} \equiv k_{sp} \quad (1)$$

where k_{sp} is the wave vector of the surface plasmon, ε_1 and ε_2 are the permittivities of air and Au, respectively, and N is an integer.

To understand the near-field behaviors of the nanofin-cavity structures, a time-averaged Poynting vector field representing the optical flow computed using the finite-difference time-domain technique (FullWAVE, Rsoft Design Group, Ossining, U.S.A.) is illustrated in Figure 2a. Strong optical flows can be

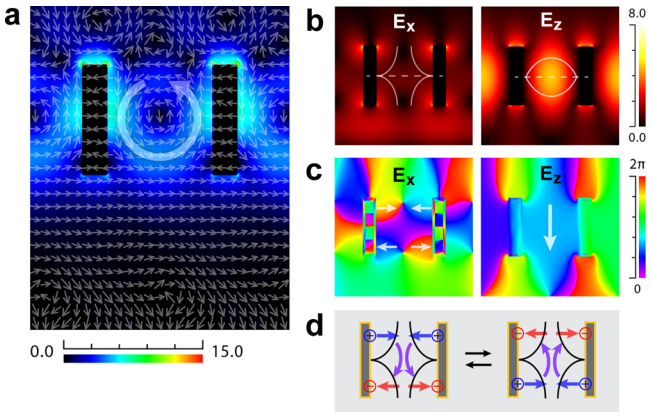

Figure 2. (a) Simulated time-averaged Poynting vector fields. The cavity parameters, incident angle, and polarization of the incident light are the same as at Point B defined in Figure 1. (b) Electric field magnitude distributions in the x- and z-direction. The density relative to free space is shown on a linear scale. (c) Electric field phase distributions in the x- and z-directions. (d) Schematic diagram of electric field directions in the nanofin cavity.

seen in the nanofin cavity, with plasmonic hot spots on the corners of the nanofins, which is evidence for the coupling of the plasmonic ridge mode and the nanofin-cavity mode. Due to the coupled mode, light turns in a loop in the cavity. As a result, the optical properties of the nanofin-cavity structure effectively change from transparent (low reflectance) to reflective (high reflectance) at the resonance wavelength. The strong optical flows in the cavity are generated from the enhanced electric field distributions in the horizontal and vertical directions, that is, x- and z-directions shown in Figure 2b. The electric field magnitude distributions in Figure 2b indicate the presence of a standing-wave resonance due to the coupling of the plasmonic hot spots with the nanofin-cavity mode. The plasmonic hot spots support antinodes on the ridges of the nanofins in the x-direction, and the strong enhancement in the cavity center supports the antinode in the z-direction, whereas the middles of the nanofins support nodes in the x- and z-directions due to the boundary conditions. The electric field phase distributions in the x- and z-directions in Figure 2c represent the directions of the electric field under resonance conditions. There is only a single phase shown in the cavities in the z-direction, whereas there is a phase variation in the x-direction. By utilizing Figure 2b,c, the electric field distributions can be identified and are

DOI: 10.1021/acsphotonics.5b00083
ACS Photonics 2015, 2, 730−737

schematically shown in Figure 2d. A symmetric mode is shown in the cavity with an even condition, supporting a single loop-turn optical flow pattern in the cavity. As a result, light will not transmit through the nanofin cavities but instead turns in a loop and becomes reflected; thus, a strong peak is observed in the reflection spectrum.

To demonstrate the different resonance modes that can be obtained by varying the cavity dimensions, Figure 3a presents

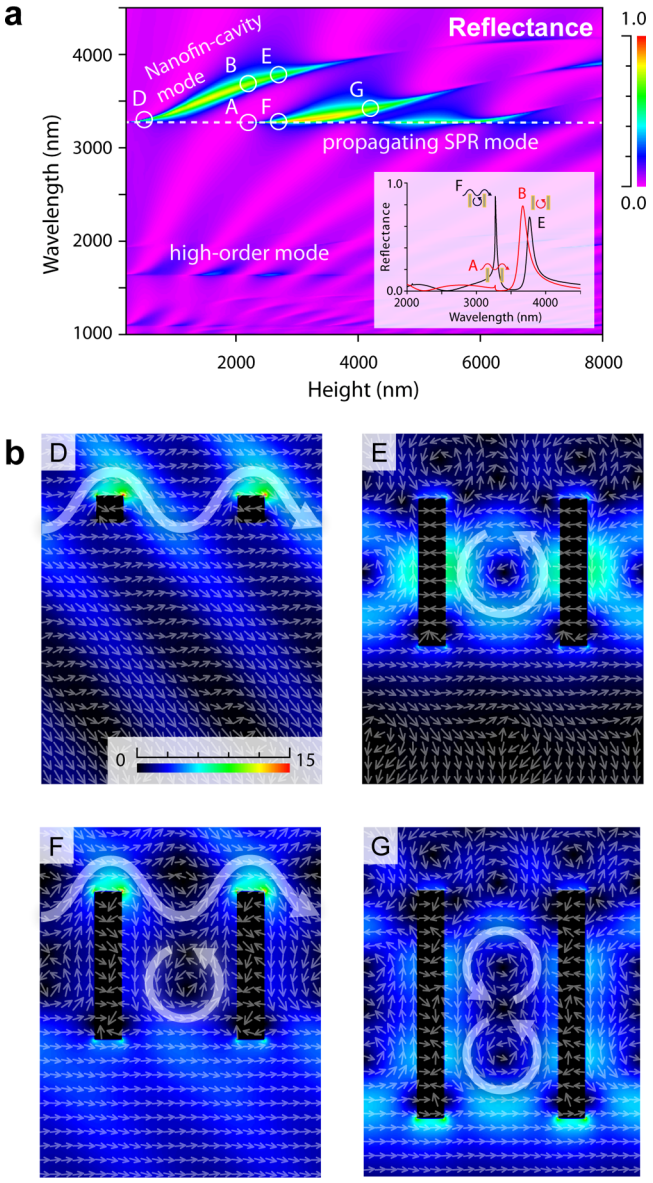

Figure 3. (a) Reflectance variation with light wavelength and cavity height exhibiting different resonance modes with periodic boundary conditions for p = 2600 nm, w = 500 nm, and t = 100 nm at θ = 15°. The inset shows the reflection spectra with h = 2200 and 2500 nm in red and black, respectively. (b) Simulated time-averaged Poynting vector fields at Points D, E, F, and G, as defined in (a).

the reflectance variation when changing both the light wavelength and the nanofin height h, with all other parameters kept constant at the values corresponding to Point B in Figure 1d (p = 2200 nm, w = 500 nm, t = 100 nm, and θ = 15°). The horizontal dashed line at λ = 3273 nm corresponds to a propagating SPR condition whose resonance wavelength is determined by the constant period of the cavities and constant incident angle (i.e., it is determined by eq 1 with N = −1). Two spectra in red and black for different nanofin heights (h = 2200 and 2500 nm, respectively) are shown in the inset of Figure 3a. Compared with the peak of the SPR mode (Point A) with a small modulation and narrow bandwidth due to the stringent excitation condition on the propagating SPR and the peak of the nanofin-cavity mode (Point B) with a large modulation and broad bandwidth (h = 2200 nm), the peak of the nanofin-cavity mode for the wavelength approaching Point A but having larger cavity height (Point F) shows a narrow-band resonance with a large modulation in reflectance. This resonance results from the coupling of the nanofin-cavity mode and SPR mode. To analyze the different modes in the nanofin cavities, the time-averaged Poynting vector fields at Points D (3289 nm), E (3770 nm), F (3275 nm), and G (3410 nm) are illustrated in Figure 3b. Point D for low-aspect-ratio cavities shows a conventional propagating SPR mode: the optical flow propagates horizontally in the x-direction above the structure or strongly transmits through the structure. The strong optical flow pattern in the cavity at point E is a result of the nanofin cavity mode, and the light turns in a loop in the cavity. Consequently, light is not transmitted through the cavity structure but is reflected at Point E. For Point F under the condition of SPR, there are a loop-turn optical flow in the cavity and a propagating optical flow above the cavity. Because of the nanofin-cavity mode for the high reflectance and the propagating SPR mode under strict excitation conditions, the peak of the coupled mode has a narrow bandwidth and large modulation at Point F. As the height of the cavity is increased, a high-order nanofin-cavity mode appears with a multiloop-turn optical flow pattern in the cavity at Point G. High-order modes of nanofin cavities with lower aspect ratios can be obtained at much shorter wavelengths, and these are demonstrated in the experiments.

A detailed discussion of the high-order nanofin-cavity modes is provided below. The resonances of the nanofin-cavity modes are related to the absorption of the structure; here, Figure 4a,b plot the resonance condition as a function of the light incident angle in the form of the absorption variation for two nanofin heights h = 5300 (rectangular nanofin cavities) and 2200 nm (square nanofin cavities) with all other parameters kept constant at the values corresponding to Point B in Figure 1d (p = 2200 nm, w = 500 nm, and t = 100 nm). The rectangular nanofin-cavity structure has four cavity modes (M1, M2, M3, and M4). The electric field directions of the different modes are schematically shown in Figure 4d (see Supporting Information). The first mode, an odd antisymmetric one (M1), appears at the longest resonance wavelength of 4071 nm, whereas the other three (M2, M3, and M4) are even symmetric higher-order modes at 3568, 3050, and 2652 nm. M2 and M4 (Figure 4a) correspond to the modes of the square nanofin-cavity structure M2′ and M4′ (Figure 4b), as indicated by their similar resonance wavelengths. These two modes in the rectangular nanofin-cavity structure exhibit a symmetric extension of the square nanofin-cavity structure. In these cavity modes of the nanofin-cavity structure, the ends of the nanofins always support antinodes at resonances. Therefore, M2′ and M4′ appear in the square nanofin-cavity structure as a result of M2 and M4 having antinodes in the middle of the nanofins, whereas M1 and M3 do not appear due to the nodes in the middles of nanofins. To satisfy the requirements for the nodes in the middles of nanofins, an Au layer can be utilized as a mirror boundary. In Figure 4c, M1′ and M3′, having similar

DOI: 10.1021/acsphotonics.5b00083
ACS Photonics 2015, 2, 730−737

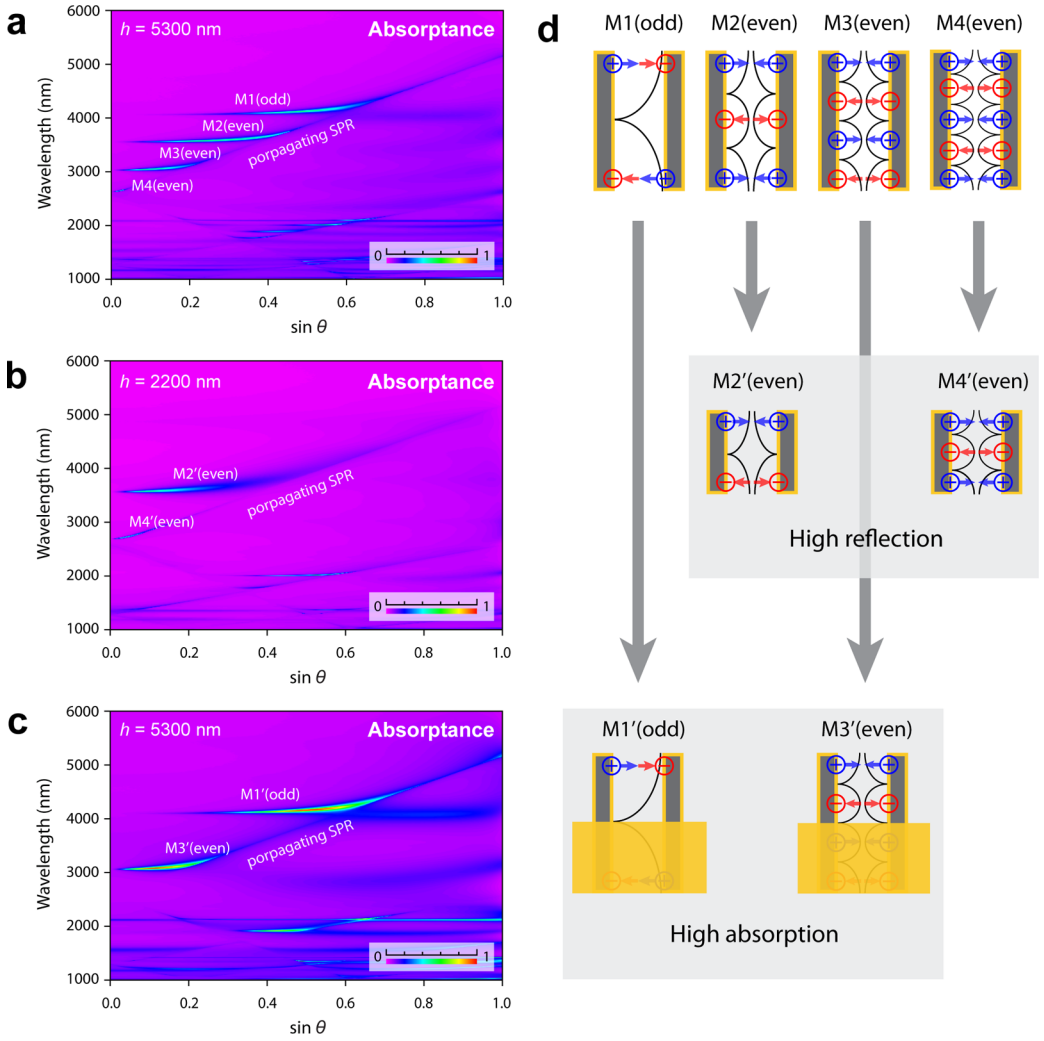

Figure 4. Dispersion diagrams showing the absorption variations of nanofin-cavity structures having (a) h = 5300 nm, (b) h = 2200 nm, and (c) nanofin-cavity structure having h = 5300 nm with the Au mirror substrate placed from the middle to the bottom of the cavities (as shown in (d)). (d) Schematic diagrams of electric field directions at resonance modes in (a), (b), and (c).

resonance wavelengths to those of M1 and M3, appear in a nanofin-cavity structure with the Au mirror at its bottom. This type of cavity forming a U is reported as a U-cavity structure.[35]

The nanofin-cavity structure was fabricated in the following steps (see Figure 5a). A silicon on insulator (SOI) substrate with a 2 μm active layer (Si), a 1 μm buried oxide layer (SiO_2), and a 400 μm handle layer (Si) was cleaned, and a photolithography resist (THMRip1800EP, Tokyo Ohka Kogyo Co., Ltd., Tokyo, Japan) was spin-coated on the device layer of the substrate. The lithography process was performed with an i-line stepper system (NSR-2205i11D, Nikon Corporation, Tokyo, Japan) to form a line-and-space resist pattern. Then, the device layer was etched by reactive ion etching (RIE-800iPB, Samco Inc., Kyoto, Japan). After the etching on the top was finished, another photolithography process with an aligner (MA200, SUSS MicroTec Group, Garching, Germany) was performed from the bottom to etch the handle layer and buried layer. Finally, the structure was sputtered (Canon Anelva Corporation, Kawasaki, Japan) with a thin (10 nm) titanium (Ti) adhesion layer, followed by the deposition of a second conformal Au layer from the top and bottom. Figure 5c shows electron microscopy images (top-view of a large area) of the fabricated nanofin-cavity structure. Supports with a width of 25 μm were placed in the direction perpendicular to the 250 μm nanofins. The optical properties of the fabricated structure having p = 4500 nm, w = 800 nm, h = 2100 nm, and t = 50 nm were ascertained by comparing the reflection spectrum measured by FT-IR spectrometer (VIR-300, JASCO, Tokyo, Japan) and simulated reflection spectrum in Figure 5b. Both zero-order reflection spectra were obtained for the same conditions, namely incident p-polarized light at an incident angle of θ = 10° in air. The simulated spectrum is in good agreement with the measured spectrum in terms of the resonance positions, bandwidths, and reflectance modulation. The about 0.1 (10%) higher reflectance in the nonresonant wavelength region results from the reflected area of the supports. A sharp and strong reflectance peak is observed at λ = 5655 nm; it has a narrow bandwidth with an FWHM of 127 nm and a reflectance larger than 0.55. The peak at λ = 5549 nm with an incident angle θ = 6° has a smaller FWHM (92 nm). The structure's performance can be further characterized by calculating the Q factor, representing the power dissipation and light confinement in the structure. The Q factor is defined as $Q = 2\pi f_r(E/P) = f_r/\Delta f$, where f_r is the resonant frequency, E is the confined light energy in the structure, P is the power dissipation, and Δf is the bandwidth of the resonance. Q is as

DOI: 10.1021/acsphotonics.5b00083
ACS Photonics 2015, 2, 730−737

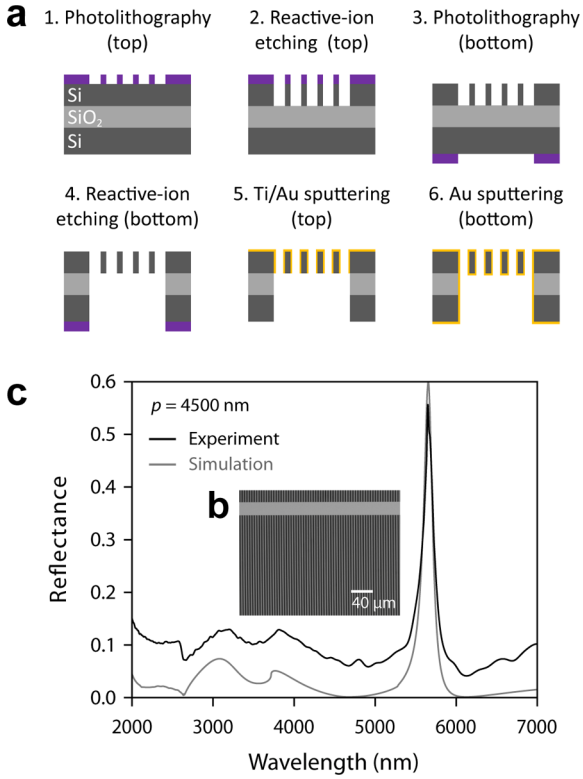

Figure 5. (a) Fabrication process of the nanofin-cavity structure. (b) An electron microscopy image of the fabricated nanofin-cavity structure showing the nanofin cavities and one support (top view). (c) Measured and simulated reflection spectra of the fabricated nanofin-cavity structure.

large as 60.3 at λ = 5549 nm in the IR region. The nanofin-cavity structure working as band-pass filters achieves among the best FWHMs and Q factors of plasmonic filters in the IR region (see Supporting Information).[25,38−46]

The tunable property of the resonance wavelength was demonstrated by fabricating cavity structures with different periods. Figure 6a depicts the reflection spectra of two nanofin-cavity structures having different periods. The increase in the cavity period from p = 3000 to 5500 nm resulted in a shift of the resonance peak from λ = 3809 to 6801 nm at θ = 10°. Reflectance peaks with much shorter resonance wavelengths in the NIR region could be obtained by using the same nanofin-cavity structures with high-order modes. Figure 6b,c shows the reflection spectra at θ = 65°, as measured by visible/NIR spectrophotometry (V-670, JASCO, Tokyo, Japan). For the same large-scale cavity period (p = 4500 nm), the reflectance peaks at λ = 1457 and 1238 nm, which are much shorter than the cavity period, have very narrow bandwidths (FWHM = 35 and 24 nm). The resonance wavelengths with different cavity periods (p = 4500 and 5500 nm) match the simulated resonance wavelengths and demonstrate the tunable property in the NIR region. The high-order modes can thus possibly alleviate the difficulty of fabricating nanostructures for short resonance wavelengths.

Due to the tunable and narrow-band reflectance property of the nanfin-cavity structure, a narrow-band filtering window in the fingerprint region can be designed and used to discriminate organic molecules. The narrow-band filtering window should be designed for a specific wavelength for which the targeted molecule has the largest absorption difference with other molecules. Under this condition, a simple photodetector in combination with the optimized filter could be used to discriminate the targeted molecule. In Figure 6d,e, the discrimination of an organic solvent (acetone) from other common solvents (ethanol, isopropyl alcohol, ethylene glycol, heptane, octane, cyclohexane, and water) is demonstrated. The reflectance spectra of water, ethanol, and acetone shown in Figure 6d were obtained using a liquid cell equipped with two 150-μm-thick glass windows separated with a distance of 100 μm. The liquid cell was inserted in front of a gold mirror. The resonance wavelength (3809 nm) of the nanofin-cavity structure having p = 3000 nm corresponds to the wavelength for which acetone and other major solvents have their largest difference in reflectance. As shown in Figure 6e, by replacing the gold mirror with the nanofin-cavity structure, the reflectance spectra of water and ethanol show no obvious peaks and have low reflectance values of 0.16 and 0.11, respectively. In contrast, the reflectance spectrum of acetone taken with the nanofin structure exhibits the peak corresponding to the resonance wavelength at 3809 nm with a high reflectance value of 0.47. The inset of Figure 6e shows the reflectance values obtained with different organic solvents at the resonance wavelength of 3809 nm. Comparing to acetone having the high reflectance value of 0.47, alcohols, including ethanol, isopropyl alcohol, and ethylene glycol, show reflectance values from 0.09 to 0.11 and alkanes, including heptane, octane, and cyclohexane, show reflectance values from 0.29 to 0.33.

To further clarify the spectral features of the nanofin-cavity structure, reflection spectra measured at various incident angles θ = 4−12° are presented in Figure 7a. Due to the coupling of the nanofin cavities and SPR, the resonance peak is not only sharp, but also has an angular dependence. This property could be potentially exploited to realize angle-controlled optical switching. It is noted that the light reflectance of nanofin-cavity structures results from the loop-turn optical flow, which is supported by the coupling of standing-wave surface plasmons in both vertical (nanofin plane) and horizontal direction (plane perpendicular to the nanofins). To excite the standing-wave surface plasmons in both directions, the wave vector of incident light should have a strong enough component on both directions. When light is incident on the nanofin-cavity structure with a small angle, the loop-turn optical flow cannot be supported due to the small component of the wave vector on the horizontal direction. Therefore, the reflectance decreases for small incident angles due to the weak optical flow (see Supporting Information). For an incident angle above 10°, the reflectance reaches a value larger than 0.5. Figure 7b shows reflectance variation for different incident angles at a fixed wavelength λ = 5710 nm. By varying the angle within 2°, a high reflectance larger than 0.55 (55%) representing the ON state can be switched to a low reflectance smaller than 0.1 (10%) representing the OFF state. These values suggest a possible approach for optical switching in the IR region. Due to the angular dependence and sharp resonance peak of the coupling of the nanofin cavities to SPR, light can only be reflected effectively under specific conditions.

In summary, the fabricated nanofin-cavity structure exhibits tunable, strong, and sharp reflectance peaks in a wide range of the IR region. The optical flows in the nanofin cavities supported by the cavity mode turn light in a loop; as a result, the optical properties change from high transmittance to high reflectance at the resonance wavelength. Measurements of the

DOI: 10.1021/acsphotonics.5b00083
ACS Photonics 2015, 2, 730−737

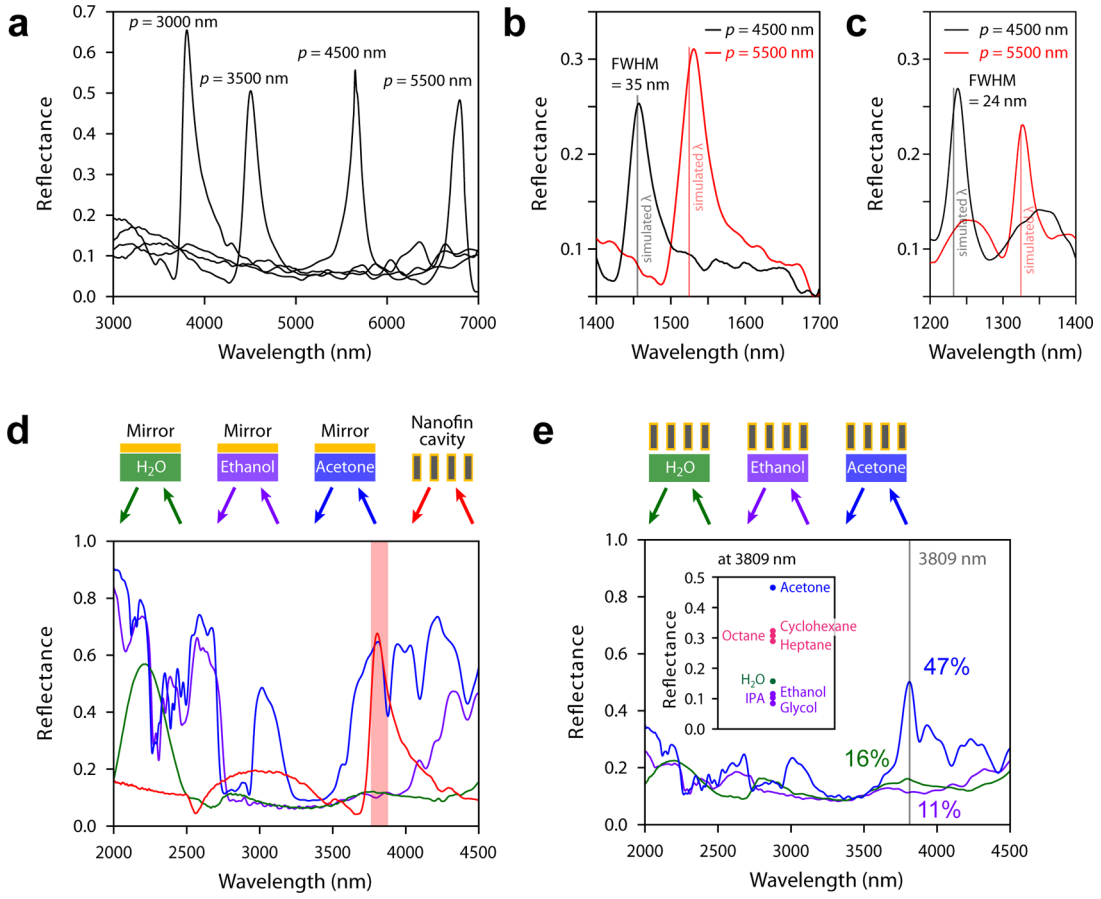

Figure 6. Measured reflection spectra of nanofin-cavity structure having (a) the periods of p = 3000, 3500, 4500, and 5500 nm in the IR region and (b, c) the periods of p = 4500 and 5500 nm in the NIR region with high-order modes. (d) Measured reflection spectra for liquid cells containing water, ethanol, and acetone inserted in front of Au mirrors, together with the reflection spectrum of the nanofin-cavity structure with p = 3000 nm. (e) Measured reflection spectra for liquid cells containing water, ethanol, and acetone in front of the nanofin-cavity structure. The inset of (e) shows the reflectance values obtained with different solvents at λ = 3809 nm.

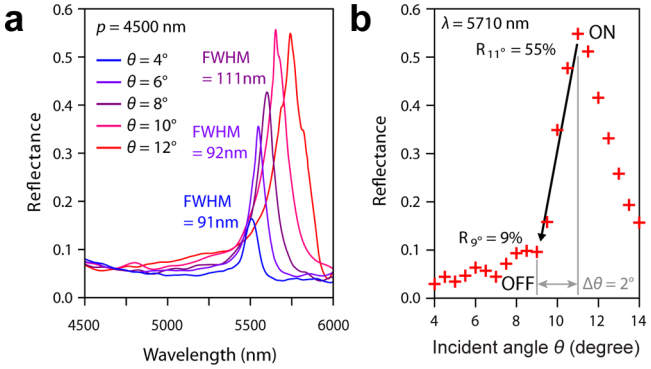

Figure 7. (a) Measured reflection spectra of nanofin-cavity structure having the period p = 4500 nm with incident angle θ = 4−12°. (b) Measured reflectance variation with incident angle θ = 4−14° at a fixed wavelength λ = 5710 nm.

fabricated structure demonstrated the reflectance peaks of different modes with FWHMs of 24, 35, and 92 nm at resonance wavelengths λ of 1238, 1457, and 5549 nm from the NIR to IR region using different order modes and also tunability by varying the period of the nanofins. This structure can be used as a reflected band-pass plasmonic filter with narrow bandwidths in the IR region. Due to the coupling of the nanofin cavities to propagating SPR, the reflectance can be switched from 55% to 9% by varying the angle of incidence within 2°. Such angle-controlled reflectance is promising for optical switching. Although this study concentrated on the filtering and switching properties in the IR and NIR region, which are of major interest for studying the fingerprint region and biosensing, the nanofin-cavity structure can be designed to suit the requirements of many other applications in the visible to the terahertz regions.

METHODS

Simulation Details. The simulations of reflectance, transmittance, and absorptance spectra were performed with the rigorous coupled-wave analysis (DiffractMOD, Rsoft Design Group, Ossining, U.S.A.). The Poynting vector fields, electric energy density distributions, electric field magnitude distributions, and electric field phase distributions were computed using the finite-difference time-domain technique (FullWAVE, Rsoft Design Group, Ossining, U.S.A.). The complex permittivity of Au is described by the Lorentz−Drude dispersion model. Periodic boundary conditions are applied in the x-direction and perfectly matched layer (PML) boundary conditions are applied in the z-direction at the top and the bottom of the simulated domain. All intensities in figures were shown relative to that of the incident wave.

DOI: 10.1021/acsphotonics.5b00083
ACS Photonics 2015, 2, 730−737

■ ASSOCIATED CONTENT

Supporting Information

Comparison table of filters based on nanostructures in infrared region, dispersion diagrams of the nanofin-cavity structure, and discussion on the resonance conditions of the high-aspect-ratio nanofin-cavity structures and the effect of the light incident angle. The Supporting Information is available free of charge on the ACS Publications website at DOI: 10.1021/acsphotonics.5b00083.

■ AUTHOR INFORMATION

Corresponding Author

*E-mail: jean@mech.t.u-tokyo.ac.jp.

Notes

The authors declare no competing financial interest.

■ ACKNOWLEDGMENTS

This work was supported by Grants-in-Aid for Scientific Research (26289013, 25630019), Grants-in-Aid for JSPS Fellows, and JSPS Core-to-Core Program (Advanced Research Networks type A) from the Ministry of Education, Culture, Sports, Science and Technology (MEXT), Japan.

■ REFERENCES

(1) Henzie, J.; Lee, M. H.; Odom, T. W. Multiscale patterning of plasmonic metamaterials. *Nat. Nanotechnol.* **2007**, *2*, 549.

(2) Lal, S.; Link, S.; Halas, N. J. Nano-optics from sensing to waveguiding. *Nat. Photonics* **2007**, *1*, 1641−648.

(3) Ma, R.-M.; Oulton, R. F.; Sorger, V. J.; Zhang, X. Plasmon lasers: coherent light source at molecular scales. *Laser Photon. Rev.* **2007**, *7*, 1−21.

(4) Vesseur, E. J. R.; Waele, R. D.; Lezec, H. J.; Atwater, H. A.; García de Abajo, F. J.; Polman, A. Surface plasmon polariton modes in a single-crystal Au nanoresonator fabricated using focused-ion-beam milling. *Appl. Phys. Lett.* **2008**, *92*, 083110.

(5) Gao, H.; Henzie, J.; Lee, M. H.; Odom, T. W. Screening plasmonic materials using pyramidal gratings. *Proc. Natl. Acad. Sci. U.S.A.* **2008**, *105*, 20146−20151.

(6) Stewart, M. E.; Anderton, C. R.; Thompson, L. B.; Maria, J.; Gray, S. K.; Rogers, J. A.; Nuzzo, R. G. Nanostructured plasmonic sensors. *Chem. Rev.* **2008**, *108*, 494−521.

(7) Ye, J.-S.; Matsuyama, N.; Kanamori, Y.; Hane, K. Silicon suspended resonant grating filters fabricated from a silicon-on-insulator wafer. *IEEE Photon. Technol. Lett.* **2008**, *20*, 851−853.

(8) de Waele, R.; Burgos, S. P.; Polman, A.; Atwater, H. A. Plasmon dispersion in coaxial waveguides from single-cavity optical transmission measurements. *Nano Lett.* **2009**, *9*, 2832−2837.

(9) Sorger, V. J.; Oulton, R. F.; Yao, J.; Bartal, G.; Zhang, X. Plasmonic Fabry-Pérot nanocavity. *Nano Lett.* **2009**, *9*, 3489−3493.

(10) Atwater, H. A.; Polman, A. Plasmonics for improved photovoltaic devices. *Nat. Mater.* **2010**, *9*, 205−213.

(11) Zhou, W.; Odom, T. W. Tunable subradiant lattice plasmons by out-of-plane dipolar interactions. *Nat. Nanotechnol.* **2011**, *6*, 423−427.

(12) Halas, N. J.; Lal, S.; Chang, W.-S.; Link, S.; Nordlander, P. Plasmons in strongly coupled metallic nanostructures. *Chem. Rev.* **2011**, *8*, 3913−3961.

(13) Barnes, W. L.; Dereux, A.; Ebbesen, T. W. Surface plasmon subwavelength optics. *Nature* **2003**, *424*, 824−830.

(14) Schuller, J. A.; Barnard, E. S.; Cai, W.; Jun, Y. C.; White, J. S.; Brongersma, M. L. Plasmonics for extreme light concentration and manipulation. *Nat. Mater.* **2010**, *9*, 193−204.

(15) García de Abajo, F. J. Colloquium: Light scattering by particle and hole arrays. *Rev. Mod. Phys.* **2007**, *79*, 1267−1290.

(16) Xu, T.; Wu, Y.-K.; Luo, X.; Guo, L. J. Plasmonic nanoresonators for high-resolution colour filtering and spectral imaging. *Nat. Commun.* **2010**, *1*, 59.

(17) Zhang, Q.; Huang, X.-G.; Lin, X.-S.; Tao, J.; Jin, X.-P. A subwavelength coupler-type MIM optical filter. *Opt. Express* **2009**, *17*, 7549−7554.

(18) Chen, Q.; Cumming, D. R. S. High transmission and low color cross-talk plasmonic color filters using triangular-lattice hole arrays in aluminum films. *Opt. Lett.* **2010**, *18*, 14056−14062.

(19) Lee, J.; Lu, F.; Belkin, M. A. Broadly wavelength tunable bandpass filters based on long-range surface plasmon polaritons. *Opt. Lett.* **2011**, *36*, 3744−3746.

(20) Sun, Z.; Zuo, X. Tuning resonant optical transmission of metallic nanoslit arrays with embedded microcavities. *Opt. Lett.* **2009**, *34*, 1411−1413.

(21) Neutens, P.; Lagae, L.; Borghs, G.; Van Dorpe, P. Plasmon filters and resonators in metal-insulator-metal waveguides. *Opt. Express* **2012**, *20*, 3408−3423.

(22) Rajasekharan, R.; Balaur, E.; Minovich, A.; Collins, S.; James, T. D.; Djalalian-Assl, A.; Ganesan, K.; Tomljenovic-Hanic, S.; Kandasamy, S.; Skafidas, E.; Neshev, D. N.; Mulvaney, P.; Roberts, A.; Prawer, S. Filling schemes at submicron scale: Development of submicron sized plasmonic colour filters. *Sci. Rep.* **2014**, *2*, 6435.

(23) Yang, C.; Shen, W.; Zhang, Y.; Peng, H.; Zhang, X.; Liu, X. Design and simulation of omnidirectional reflective color filters based on metal-dielectricmetal structure. *Opt. Express* **2014**, *22*, 11348−11391.

(24) Lin, X.-S.; Huang, X.-G. Tooth-shaped plasmonic waveguide filters with nanometeric sizes. *Opt. Lett.* **2008**, *33*, 2874−2876.

(25) Cheng, C.-W.; Abbas, M. N.; Chang, Z.-C.; Shih, M. H.; Wang, C.-M.; Wu, M. C.; Chang, Y.-C. Angle-independent plasmonic infrared band-stop reflective filter based on the Ag/SiO_2/Ag T-shaped array. *Opt. Lett.* **2011**, *36*, 1440−1422.

(26) Wang, C.-M.; Tsai, D. P. Plasmonic infrared bandstop reflective filter. *IEEE J. Sel. Top. Quantum Electron.* **2013**, *19*, 4601005.

(27) Foresi, J. S.; Villeneuve, P. R.; Ferrera, J.; Thoen, E. R.; Steinmeyer, G.; Fan, S.; Joannopoulos, J. D.; Kimerling, L. C.; Smith, H. I.; Ippen, E. P. Photonic-bandgap microcavities in opticalwaveguides. *Nature* **1997**, *390*, 143−145.

(28) Md Zain, A. R.; Johnson, N. P.; Sorel, M.; De La Rue, R. M. Ultra high quality factor one dimensional photonic crystal/photonic wire micro-cavities in silicon-on-insulator (SOI). *Opt. Express* **2008**, *16*, 12084−12809.

(29) Bozhevolnyi, S. I.; Volkov, V. S.; Devaux, E.; Laluet, J.-Y.; Ebbesen, T. W. Channel plasmon subwavelength waveguide components including interferometers and ring resonators. *Nature* **2006**, *440*, 508−511.

(30) Seo, M.-K.; Kwon, S.-H.; Ee, H.-S.; Park, H.-G. Full three-dimensional subwavelength high-Q surface-plasmon-polariton cavity. *Nano Lett.* **2009**, *9*, 4078−4082.

(31) Min, B.; Ostby, E.; Sorger, V.; Ulin-Avila, E.; Yang, L.; Zhang, X.; Vahala, K. High-Q surface-plasmon-polariton whispering-gallery microcavity. *Nature* **2009**, *457*, 455−459.

(32) Della Valle, G.; Søndergaard, T.; Bozhevolnyi, S. I. High-Q plasmonic resonators based on metal split nanocylinders. *Phys. Rev. B* **2009**, *80*, 235405.

(33) Miyazaki, H. T.; Ikeda, K.; Kasaya, T.; Yamamoto, K.; Inoue, Y.; Fujimura, K.; Kanakugi, T.; Okada, M.; Hatade, K.; Kitagawa, S. Thermal emission of two-color polarized infrared waves from integrated plasmon cavities. *Appl. Phys. Lett.* **2008**, *92*, 141114.

(34) Inoue, T.; De Zoysa, M.; Asano, T.; Noda, S. Filter-free nondispersive infrared sensing using narrow-bandwidth mid-infrared thermal emitters. *Appl. Phys. Express* **2014**, *7*, 012103.

(35) Ho, Y.-L.; Portela, A.; Lee, Y.; Maeda, E.; Tabata, H.; Delaunay, J.-J. Hollow plasmonic U-cavities with high-aspect-ratio nanofins sustaining strong optical vortices for light trapping and sensing. *Adv. Opt. Mater.* **2014**, *2*, 522−528.

(36) Ho, Y.-L.; Lorendel, G.; Delaunay, J.-J. Plasmonic hybrid cavity-channel structure for tunable narrow-band optical absorption. *IEEE Photon. Technol. Lett.* **2014**, *26*, 1979.

(37) Raether, H. *Surface Plasmons on Smooth and Rough Surfaces and on Gratings*; Springer: Berlin; Heidelberg, 1988.

(38) Vial, B.; Commandré, M.; Demésy, G.; Nicolet, A.; Zolla, F.; Bedu, F.; Dallaporta, H.; Tisserand, S.; Roux, L. Transmission enhancement through square coaxial aperture arrays in metallic film: when leaky modes filter infrared light for multispectral imaging. *Opt. Lett.* **2014**, *39*, 4723−4726.
(39) Yan, H.; Low, T.; Zhu, W.; Wu, Y.; Freitag, M.; Li, X.; Guinea, F.; Avouris, P.; Xia, F. Damping pathways of mid-infrared plasmons in graphene nanostructures. *Nat. Photonics* **2013**, *7*, 394−399.
(40) Wang, C.; Zhang, Q.; Song, Y.; Chou, S. Y. Plasmonic bar-coupled dots-on-pillar cavity antenna with dual resonances for infrared absorption and sensing: performance and nanoimprint fabrication. *ACS Nano* **2014**, *8*, 2618−2624.
(41) Cheng, C.-W.; Abbas, M. N.; Chiu, C.-W.; Lai, K.-T.; Shih, M. H.; Chang, Y.-C. Wide-angle polarization independent infrared broadband absorbers based on metallic multisized disk arrays. *Opt. Express* **2012**, *20*, 10376−10381.
(42) Abbas, M. N.; Cheng, C.-W.; Shih, M. H.; Chang, Y.-C. An omni-directional mid-infrared tunable plasmonic polarization filter. *Nanotechnology* **2012**, *23*, 444007.
(43) Sakat, E.; Vincent, G.; Ghenuche, P.; Bardou, N.; Dupuis, C.; Collin, S.; Pardo, F.; Haïdar, R.; Pelouard, J.-L. Free-standing guided-mode resonance band-pass filters: from 1D to 2D structures. *Opt. Express* **2012**, *20*, 13082−13090.
(44) Le Perchec, J.; Espiau de Lamaestre, R.; Brun, M.; Rochat, N.; Gravrand, O.; Badano, G.; Hazart, J.; Nicoletti, S. High rejection bandpass optical filters based on sub-wavelength metal patch arrays. *Opt. Express* **2011**, *19*, 15720−15731.
(45) Collin, S.; Vincent, G.; Haïdar, R.; Bardou, N.; Rommeluère, S.; Pelouard, J.-L. Nearly perfect Fano transmission resonances through nanoslits drilled in a metallic membrane. *Phys. Rev. Lett.* **2010**, *104*, 027401.
(46) Foley, J. M.; Young, S. M.; Phillips, J. D. Narrowband mid-infrared transmission filtering of a single layer dielectric grating. *Appl. Phys. Lett.* **2013**, *103*, 071107.

DOI: 10.1021/acsphotonics.5b00083
ACS Photonics 2015, 2, 730−737